Highlights

Earthquake-induced landslides coupled to fluvial incision in Andean Patagonia: inferring their effects on landscape at geological time scales

Bastian Morales, Elizabet Lizama, Marcelo Somos-Valenzuela, Diego Rivera, Chen Ningshen

- During the year 2007 the Liquiñe-Ofqui Fault System (LOFS) showed its destructive power in Andean Patagonia, causing a 6.2 Mw earthquake in the Aysén Fjord leading to over 500 landslides with volumes reaching 12 Mm^3.
- We implemented a landscape evolution model to study co-seismic landslide erosion coupled to fluvial incision, in order to understand the long-term effects on the Aysén Fjord Landscape of the LOFS seismic cycle.
- Based on our analysis, we propose that the LOFS exerts primary control over landscape erosion and sediment generation in Andean Patagonia.

Earthquake-induced landslides coupled to fluvial incision in Andean Patagonia: inferring their effects on landscape at geological time scales

Bastian Morales[a,b], Elizabet Lizama[a,b], Marcelo Somos-Valenzuela[a,c,1], Diego Rivera[d], Chen Ningshen[e]

[a] *Butamallin Research Center for Global Change, University of La Frontera, Temuco 4780000, Chile*
[b] *Faculty of Agricultural Engineering, Universidad de Concepción, Av. Vicente Mendez 595, Chillan, Chile*
[c] *Department of Forest Sciences, Faculty of Agriculture and Environmental Sciences, University of La Frontera, Temuco 4780000, Chile*
[d] *Facultad de Ingeniería, Universidad del Desarrollo, Avenida Plaza 600, Santiago, Chile*
[e] *Key Lab of Mountain Hazards and Surface Process, Institute of Mountain Hazards and Environment, Chinese Academy of Sciences, Chengdu 610041, China*

Abstract

Earthquakes can deeply erode the mountainous landscape through co-seismic landslides, generating large amounts of sediment and debris that are then transported and distributed by rivers, controlling the landscape evolution. We can observe this influence in the Liquiñe Ofqui Fault System (LOFS), an active intra-arc fault system extending hundreds of kilometers through the Andes in Chilean Patagonia. For example, on April 21, 2007, a 6.2 Mw earthquake in the Aysén Fjord triggered over 500 landslides with volumes reaching 12-20 Mm^3. Although there is a well-defined seismic cycle, no study has focused on the effects of co-seismic landslides and sedimentary dynamics on the evolution of this mountainous landscape. In this research, we seek to improve the long-term understanding of the interaction between landslides and fluvial incisions in this segment of the Andes. For this reason, we implemented the Landlab-HyLands landscape evolution model (LEM), a hybrid landscape evolution model that allows modeling landslide activity

[⋆1] Corresponding author at:
Email address: marcelo.somos@ufrontera.cl (Marcelo Somos-Valenzuela)

coupled to fluvial incision. We consider the landslides that occurred during the 2007 earthquake as a precedent and simulate nine scenarios of ten seismic cycles over 21,000 years based on the 2100-year seismic cycle of the Holocene documented in this region. We further used multiple uplift rates, sediment erodibility, and m/n constant ratios associated with the current power law to assess this parameterization's impact on the landscape. According to our results, landslides are a fundamental mechanism in the landscape's evolution in this region. Deposits derived from landslides can create transitory landscape forms that can intervene in fluvial dynamics. According to our simulations, a significant part of the landslide sediment can remain on the slopes for thousands of years. We identified that parameterization considerably impacts the evolutionary response of the landscape in the evaluated time scale. Low m/n ratios can generate a different evolutionary response than other scenarios because the slopes are constantly driven towards their threshold angle, intensifying the interaction between landslides and fluvial incisions. Based on our analysis and considering the historical record of the Aysen Fjord, we can explain a critical primary control of the LOFS on landscape erosion and sediment production because of the surface seismic cycle. In our study, we demonstrate how the implementation of hybrid LEM can help to infer the contribution of sediments associated with large earthquakes and to improve the understanding of the role of landslides in the evolutionary history of Andean Patagonia. However, we stress that it is essential to advance in capturing erodibility and incision parameters of the current power law in the Andes and local geomechanical information. Finally, we believe the LEM can help to deepen the knowledge of these processes in other Andean basins exposed to these geomorphological processes.

Keywords: Landslides, Patagonian Andes, Aysén Fjord, Landscape evolution, LOFS

1. Introduction

Erosion processes affect the dynamics of landscapes and ecosystems, representing a threat to vegetation, soils, and habitats by altering infiltration rates and surface runoff, but also are a hazard to human life and infrastructure. In this sense, landslides can be the primary erosion mechanism in the mountains and complex topography environments (Broeckx et al., 2020; Hovius et al., 1997). Specifically, landslides associated with large earthquakes

can generate erosion and deposition patterns with the capacity to change the shape of the landscape on different temporal and spatial scales (Crozier, 2010; Shobe et al., 2021). The extensive sediment volumes generated by landslides are transported by fluvial channels from mountain basins to the ocean (Milliman and Meade, 1983). Also, sediment release produces incisions in the bedrock, generating a chain reaction that 1) reduces the surrounding slopes' base level, 2) makes slopes collapse due to the mass lost, obstructing rivers with sediment and impeding further incisions in the bedrock until the sediments derived from landslides are evacuated from the system (Campforts et al., 2020a; Korup et al., 2010; Larsen and Montgomery, 2012).

Co-seismic landslides, i.e., landslides that occur during or shortly after the earthquake, can generate large volumes of sediments and rubble derived from the soil and bedrock of mountain chains (Fan et al., 2019). Much of the material released remains on slopes or in secondary channels for a long time, forming deposits, while the rest is transferred directly to rivers, where it can be transported by the current (Dai et al., 2021). After earthquakes, it is common to see an increase in sediment discharge in mountain rivers (Hovius et al., 2011; Wang et al., 2015), although there are also exceptions (Tolorza et al., 2019). It has been identified that this period of high erosion is generally short, typically lasting less than a decade, resulting in significant volumes of sediment remaining in the mountains after sediment discharges have returned to normal levels (Francis et al., 2022). This is because the sediment generated by co-seismic landslides is too thick to be transported in suspension. This sediment is transported through bedload processes and is believed to remain in the landscape for hundreds of years (Francis et al., 2022). For example, it has been empirically estimated that sediment from the 1999 Chi-Chi earthquake in Taiwan could take between 250 and 600 years to be completely evacuated from the landscape (Yanites et al., 2010). Furthermore, dating in the Pokhara region of Nepal suggests that river systems can reprocess sediments from large earthquakes over several hundred years (Schwanghart et al., 2016; Stolle et al., 2019). Recently, attempts have been made to assess the fate of sediments derived from co-seismic landslides after ten years of the seismic event (Dai et al., 2021; Francis et al., 2022). However, what happens to sediments derived from co-seismic landslides on time scales of centuries or millennia is still poorly understood, as how these processes modify mountain landscapes.

Landscape evolution models (LEM) have been widely used to study landscape changes in response to tectonics and climate change and their complex

interactions. Advances in these models have allowed for incorporating different modules, which simulate the interaction between landslides and fluvial processes at different scales. One approach to test and calibrate these models involves "natural experiments," which are case study sites defined by various criteria. First, landscape evolution is mainly controlled by a critical driver (such as current cutting or rapid transport along slopes); second, initial conditions are well known or can be inferred with sufficient detail; and third, there are restrictions available for changes over time in the studied area (Tucker, 2009).

In the Andes of southern Chile, the subduction of the Nazca plate under South America causes an extensive and active system of intra-arc faults called the Liquiñe Ofqui Fault System (LOFS), which extends for 1200 km between 39–47 ° S. This fault system, since at least the Miocene, has been the primary tectonic process along the Chilean subduction margin (Cembrano et al., 1996; Hervé et al., 2017). On April 21, 2007, the LOFS showed its destructive power, causing a shallow earthquake of 6.2 Mw in the Aysén Fjord and triggering more than 500 landslides with volumes reaching 12 Mm^3 (Naranjo et al., 2009; Sepúlveda et al., 2010). Subsequently, analysis of the historical record using sediment cores shows a return period of seismic activity in approximately 2100 years in the Aysén Fjord (Wils et al., 2018).

The history of earthquakes and large landslides makes the Aysén Fjord an exciting area to decipher the dynamics of sediments derived from landslides on various time scales. It also allows us to understand how landslide erosion coupled with fluvial incision influences the evolution of a tectonically active landscape. Thus, we conducted an experimental application in the Aysén fjord of Chilean Patagonia of the Landlab-Hylands model. This hybrid landscape evolution model can simulate landslide erosion and subsequent fluvial transport. Via this landscape evolution model, we intended to understand: What sediment dynamic arises after a period of intense co-seismic landslides? How will the landscape of the Fjord of Aysén respond to time scales after a series of stochastic co-seismic landslides?

2. Study area

The Aysén Fjord is located south of the subduction margin between the Nazca and South American plates (Figure 1). In this segment of the Andes, plate subduction form the Liquiñe-Ofqui Fault System (LOFS) (Cembrano et al., 1996; Hervé et al., 2017). This dextral strike-slip fault is the main

morpho-structural feature of the area, extending for around 1200 km and controlling much of the volcanic activity in southern Chile. The geology of this region corresponds mainly to intrusive diorite-granite rocks of the Meso-Cenozoic age belonging to the North Patagonian Batholith (NPB). Also, Paleozoic metamorphic rocks and Quaternary volcanic rocks of basalt and andesite composition are present. The study zone has notable U-shaped valleys carved by Quaternary glacial erosion, currently filled by alluvial, fluvial, and volcanic deposits (Villalobos et al., 2020). The Aysén Fjord has a detailed record of seismic activity occurring during the last 12,000 years. The stratigraphic record can be found in marine sediments from erosion caused by at least six earthquakes associated with the LOFS (Wils et al., 2018). In 2007 the Aysén Fjord saw another event in this seismic cycle, as the epicenter of an Mw 6.2 earthquake at a depth of 10 km (Sepúlveda et al., 2010). This surface seismic activity caused in the epicenter area over 500 landslides in exceptionally shallow soil, rock slides, rock falls, debris flows, and rock avalanches of up to 12 Mm^3 (Sepúlveda et al., 2010; Villalobos et al., 2020).

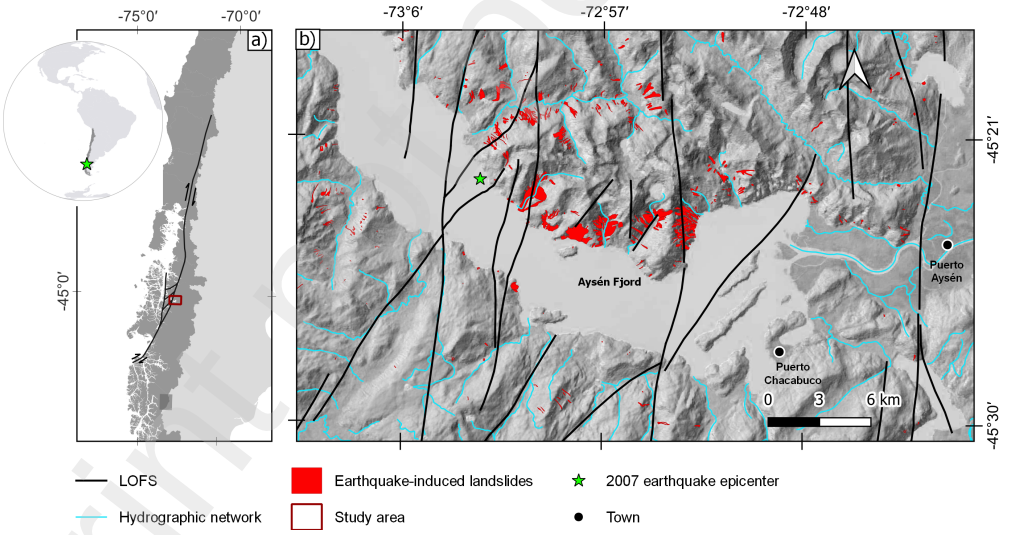

Figure 1: Study area. Polygons represent landslides associated to the Aysén earthquake, 2007.

3. Methodology

3.1. Landscape evolution model

Numerical modeling was done via Landlab, which combines a group of numerical tools to model land surface processes via the Python programming language. In our study, we used the HyLands landscape evolution model recently implemented in Landlab to simulate erosion by landslide (Campforts et al., 2020a, 2022). HyLands treats erosion and landslide earth deposits deterministically, but it uses a stochastic focus to calculate the occurrence of landslides. The HyLands model simulates deep gravitational landslides that simultaneously erode the sediment layer and the bedrock. Hylands represent the landscape as a rock surface covered by a regolith layer, varying in space and time (Campforts et al., 2020a, 2022). The evolution over time of the topographic elevation η, the elevation of the bedrock surface R, and the thickness of the moving regolith H is determined considering the following mass balance equation:

$$\frac{\partial \eta}{\partial t} = \frac{\partial R}{\partial t} + \frac{\partial H}{\partial t} \tag{1}$$

where the first term is defined as:

$$\frac{\partial R}{\partial t} = U - E_{r_{fluv}} - E_{r_{ls}} \tag{2}$$

and the second:

$$\frac{\partial H}{\partial t} = (\frac{1}{1-\phi_{sed}})(D_{s_{ls}} + D_{s_{fluv}} - E_{s_{ls}} - E_{s_{fluv}}) - \nabla \cdot q_s \tag{3}$$

In the equation, the rate of uplift of the surface regarding the base level is defined by U [LT^{-1}] and the porosity of the sediment by ϕ_{sed}. For its part, E_r [LT^{-1}] describes the rate of fluvial bedrock erosion as a volume flow per unit area, while E_s [LT^{-1}] represents the sediment entrainment and D_s [LT^{-1}] the fluvial deposition flux. The term q_s [L^2T^{-1}] corresponds to the flow of sediments associated with fluvial transport. The landslide causes bedrock erosion E_r, sediment entrainment E_s and deposition as volumetric flow per area D_s. HyLands calculates fluvial bedrock incision, sediment transport, and deposition using the SPACE model (Shobe et al., 2017), where Eq. (4) represents sediment entrainment, while Eq. (5) represents bedrock erosion:

$$E_{s_{fluv=K_s q S^n (1-e^{-H/H*fluv})}} \tag{4}$$

$$E_{r_{fluv}} = K_r q S^n e^{-H/H*fluv} \tag{5}$$

K_s and K_r [L^{-1}] are the erodibility constants for sediments and rocks, respectively. Here, q represents the discharge of water per unit width, we calculate this as $q = K_q A^m$, where k_q is a coefficient that is part of K_s and K_r. The parameter m is the exponent of the drainage area, S corresponds to the slope of the channel [L L^{-1}] and n is the exponent of the slope (Campforts et al., 2022). We calculate the sediment deposition flux as Davy and Lague (2009):

$$D_{s_{fluv}} = \frac{Q_{sfluv}}{Q} V \tag{6}$$

where D_s is the deposition flux, Q_s represents the volumetric discharge of sediment, Q is the volumetric discharge of water, and V is the effective sedimentation rate. Culmann's theory gives the probability of a slope failure occurring at a location (x, y) (Culmann, 1875), which defines that the probability of failure depends on the relationship between the height of the slope H_s and the height of the maximum stable slope H_c. A probabilistic Poisson model defines the temporal probability of stochastic landslides (Campforts et al., 2022). In Hylands, the spatiotemporal probability of failure for a location (x, y) is given by the following equation:

$$P_{fail} = (1 - e^t \frac{-t}{LS}) P_s(x, y). \tag{7}$$

Following Culmann's theory (Culmann, 1875), the spatial probability of failure P_s is defined as:

$$P_s = \frac{H_s}{H_c} \tag{8}$$

The maximum stable height of the slope H_c is determined through the following expression:

$$H_c = \frac{4C}{\rho g} \frac{sin\beta cos\phi}{1 - cos(\beta - \phi)} \tag{9}$$

where C corresponds to the cohesion [ML^{-1} T^{-2}], ρ is the density of the rock (ML^{-3}) established in this work in 2700 kg m^{-3}, g is the acceleration of gravity (9.81 $ms^{-}2$), β the topographic angle, and ϕ the internal friction angle of the rock. Once the landslide has occurred, the eroded bedrock volume (E_r) is calculated based on a Culmann stability model, assuming Mohr-Coulomb materials, where a fault plane with dip angle θ_c bisects the local topographic angle β, and the material internal friction angle ϕ (Densmore et al., 1998; Champel, 2002; Campforts et al., 2022). HyLands then distributes the sediments over the slope and deposits them using a nonlinear and nonlocal deposition scheme (Carretier et al., 2016; Campforts et al., 2022):

$$D_{s_{ls}} = \frac{Q_{sls}/\omega}{L} \tag{10}$$

where $D_{s_{ls}}$ corresponds to the deposition flux per area and $Q_{s_{ls}}$ is the volumetric discharge of landslide sediments and L (L), the transport distance.

3.2. Numerical experiment

We simulated ten landslide pulses over 21,000 years through Landlab-HyLands in the Aysén Fjord. We consider a landslide return period of 2100 years based on the seismic history documented in the area during the Holocene (Wils et al., 2018). To carry out the experiments, we use two essential components: BedrockLandslider, the landslide generator, and SpaceLargeScaleEroder, which simulates fluvial incision and sediment transport. Simulations were carried out on a 30 m resolution grid covering an area of 150 km^2; we use a digital elevation model (DEM) derived from Shuttle Radar Topography Mission (SRTM) v3.0.

Implementing Landlab-Hylands requires changing physical variables (described in the previous section) to model landslide erosion (area-volume and spatial-temporal scaling), incision, and fluvial transport. The sensitivity of the scenarios to the parameterization of the model was evaluated through nine experimental configurations that are detailed below: a base scenario was established, with an angle of internal friction of 30° and a cohesion of 20 kPa considering geomechanical conditions of rocks post- earthquake (Jeandet et al., 2019). The tectonic uplift rate was set at 0.135 mm/year, considering previously documented values for this region of Patagonia (Thomson et al., 2010). We adjusted the return time of the landslide in 2100 years, considering the stratigraphic record of the Aysén Fjord on the seismic activity of the

LOFS (Wils et al., 2018). We tune BedrockLandslider to simulate stochastic landslides over ten years, considering temporal landslide activity observed after earthquakes (Fan et al., 2019). The maximum size of the landslides was regulated considering the dimensions of the largest landslide triggered by the 2007 earthquake in the Fjord of Aysén, whose estimates oscillate between 12-20 Mm^3 (Sepúlveda et al., 2010; Lastras et al., 2013). We model the coarse portion of the sediment, assuming that all fine sediment is rapidly evacuated from the system during the first few years of the seismic event. This is based on the proximity of the deposits to the fjord and the dynamics observed during the 2007 (Naranjo et al., 2009) earthquake. For this reason, we established that fifty percent of the sediment was evacuated immediately in each pulse.

To regulate fluvial erosion, we assign commonly accepted erodibility values for rocks in active continental margins of 1 x 10^{-5}, for exponents m=0.5 and n=1 (Stock and Montgomery, 1999). These standard scale exponents are derived from an empirical analysis of stream incision in different bedrock using the stream power law (Stock and Montgomery, 1999). We set an erodibility constant for the soil of 1.5 x 10^{-5}, increasing by 1/3 the rock erodibility as previously implemented in natural experiments (Campforts et al., 2022). We developed nine experimental setups to assess the model's sensitivity to parameterization. From scenario 1 (parameters described above), we changed the value of the uplift rate, erodibility, and exponents of slope and drainage area (n and m, respectively). In previous studies, these parameters have been highly sensitive and thus can considerably affect landscape evolution scenarios (Tucker and Whipple, 2002; Booth et al., 2013; Harel et al., 2016; Barnhart et al., 2020; Campforts et al., 2022). To evaluate the impact of the variation of these parameters in our study area, we changed the uplift rate (U) to 0.76 mm/year (scenario 2) and 1.4 mm/year (scenario 3), according to different uplift rates reported in the region (Thomson et al., 2010; Vargas et al., 2013). We examined cases with erodibility values (K_s) of 1 x 10^{-4} (scenario 4), 1 x 10^{-3} (scenario 5), and 1 x 10^{-2} (scenario 8), which are within the typical range of K_s used in landscape evolution models (Lai and Anders, 2018; Barnhart et al., 2020). In addition, we tested different empirical values accepted in the literature for m/n ratios (Lague, 2014; Harel et al., 2016; Dulanya et al., 2022): 1:3/2:3 (scenario 7), 0.45/1 (scenario 8), and 0.7/2 (scenario 9). Every time we changed the value of these parameters (U, K_s or m/n), the rest kept the value used in scenario 1.

To compare the morphometric changes of the landscape in each scenario, a

Table 1: Landlab-HyLands parameters used for calibration.

Parameters	Description	Values
Rows	Number of grid rows	747
Columns	Number of grid columns	1779
Cell spacing (m)	Spatial grid resolution	30
Initial H (m)	Initial soil-deposit height	0
U (m/yr)	Tectonic uplift	Change according to scenario
K_r (m^{-1})	Rock erodibility constant	1.1 x 10^{-6}
K_s (m^{-1})	Soil erodibility constant	Change according to scenario
m (–)	Exponent	Change according to scenario
n (–)	Exponent	Change according to scenario
H^* (m)	Rock roughness	1
ϕ sed (–)	Soil/sediment porosity	0
$F_{f_{fluv}}$ (–)	Fraction of fine fluvial sediment remaining in suspension	0.5
Vc (myr^{-1})	Sedimentation speed in non-flooded cells	2
Vc Lake (myr^{-1})	Sedimentation speed in flooded cells	10
C (kPa)	Rock cohesion	22
ϕ (degree)	Internal friction angle	30
t_{LS} (yr)	Landslide return time	2100
δ ($\circ$)	Minimum angle for sediment depositing derived from landslides on slopes	0.01
$F_{f_{hill}}$ (–)	Fraction of fine sediment derived from slopes	0.25
ρ_{rock} (g/cm^3)	Rock density	2.7
Maximum landslide size (m^2)	Maximum number of pixels in m^2	135.000

set of topographic metrics was applied to both the current landscape and the simulated landscape after 21,000 years. We use the drain density metric, D_d [L^{-1}], calculated as the ratio of drain length to the area [m^{-1}]. We also apply the normalized river steepness (k_{sn}), which is the area-weighted upstream channel gradient: $k_{sn} = SA^{m/n}$, where A is the area of upstream drainage, S is the slope of the channel, and the ratio m/n is set to 0.45 (Whittaker, 2012; Campforts et al., 2022). To evaluate the areas of loss and gain of relief, we calculate the difference in elevation between the final topography of the simulation and the current topography. We evaluate the excess relief metric, Z_E, defined as the column of rocky material between the ground surface and an idealized topography with slopes less than or equal to a certain threshold slope angle, which in this case, we define as 30° (Blöthe et al., 2015). Finally, we developed a terrain classification to analyze the variability of landforms in each experiment through calculating geomorphons (Jasiewicz and Stepinski, 2013), a pattern recognition approach to landform classification and mapping available in SAGA GIS (Conrad et al., 2015).

4. Results

4.1. Post-earthquake sediment production and evacuation

We simulate the dynamics of sediments derived from co-seismic landslides over 21,000 years (Figure 3). Depending on the parameterization, the scenarios show significant differences in sediment production and evacuation. Landslides and their derived sediments are mainly concentrated in the mountainous block to the north of the fjord (Figures 4, 5, 6). From here, they are transported down the valleys towards the Aysen Fjord (Figures 4, 5, 6). According to our results, landslides are an effective mechanism of sediment production that increases river channel sediment load cyclically (Figure 3). However, the total volume of sediment generated between each cycle and its redistribution depends mainly on fluvial erosion (Figure 3). We observe the deposits associated with landslides form clusters of sediment that profoundly change the topography of the slopes and valleys (Figures 4, 5, 6).

We identified that increases in K_s produce quickly eroded deposits (scenarios 4, 5, and 6). This causes the sediment volume to be relatively constant over time and spatially uniform (Figure 3). When the m/n ratio decreases to a minimum (scenario 9), the volume of accumulated sediment increases almost linearly (Figure 3), because of the increase in the fluvial incision and the production of sediment by landslides. The change in the uplift rate does

not seem to significantly impact the amount of volume of sediment generated and its spatial distribution (Figure 3; scenarios 1-3)

According to our simulations, there are valleys where landslide-derived sediments are spatially connected with the ability to block channels, causing changes in drainage morphology (Figure A.9). We observed that channel avulsion is a typical process (Figure A.10). However, increases in sediment erodability can strongly limit this type of process (Figure A.10). Depending on the scenarios, regardless of the parameterization used, the sediment may remain in the domain for thousands of years, grouping on the slopes and in glacial morphologies (hanging valleys) disconnected from the main fluvial networks. According to our results, sediment redistribution is mainly regulated by erodability (K_s) and incision (n) (Figures 3, 5 and 6; scenarios 6 and 9). The strong coupling between the fluvial incision and landslides causes a substantial increase in sediment production because the slopes are continuously brought towards their threshold angle (Figures 6; scenario 9).

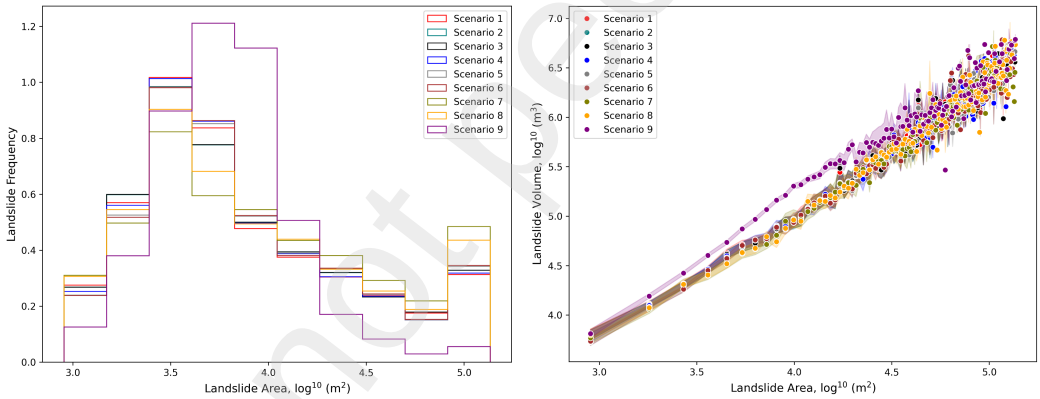

Figure 2: Left: simulated landslide area frequency density curve. Right: area-volume relationship of simulated landslides.

4.2. Geomorphological changes of the landscape

In this section, we detail the geomorphic response of the landscape at different time scales of landslide erosion coupled with fluvial incisions in the tectonically active landscape of the Aysen Fjord. We comparatively analyzed in each scenario the effects of changes in tectonic uplift, sediment erodibility and m/n ratios regarding the current landscape (Figure 7). We develop this using topographic profiles, geomorphic metrics and a topographic classification of the simulated final landscape (Figure 7).

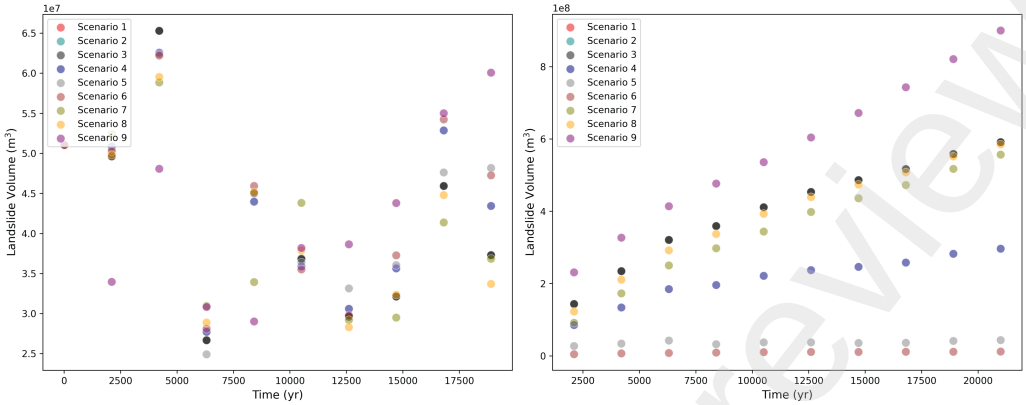

Figure 3: Left: volume of landslide deposits generated for each of the scenarios. Right: sediment volume at the end of each scenario.

Landslides can widen or steepen the valley according to the type of relief, recurrence, and incision conditions (Figure S1 in the supporting information). We identified that valleys with straight slopes because of fluvial incisions evolved into curved slopes once it triggered a landslide. Throughout the valleys, landslides alternate stochastically between slopes because of fluvial dynamics. At one end of the valley, the slopes affected by the incision reach their threshold angle, which leads to collapse. At the other extreme, deposits associated with old landslides reduce the incision, stabilizing the slope. This dynamic, repeated over time, causes the incision's mobilization across the valley's width and its widening. Landslides, when eroding preferential areas, induce an increase in incisions in areas with no deposits derived from landslides, reflecting the importance of this sedimentary material in the development of preferential erosion areas (Figure A.9).

The drainage density metric presents a notable increase compared to the current landscape in all scenarios. The lowest sensitivity of this metric is generated by the uplift scenarios (Figure 7). Comparatively, we found that drainage density is more sensitive to changes in erodibility than uplift. We note that increases of over two orders of magnitude in sediment erodibility do not produce significant changes in drainage density during the simulated period. The most significant impact on drainage density occurs when changing m/n ratios, primarily when we perform modeling under non-linear incision conditions (scenario 9).

The k_{sn} metric shows a non-linear behavior with the uplift and sediment

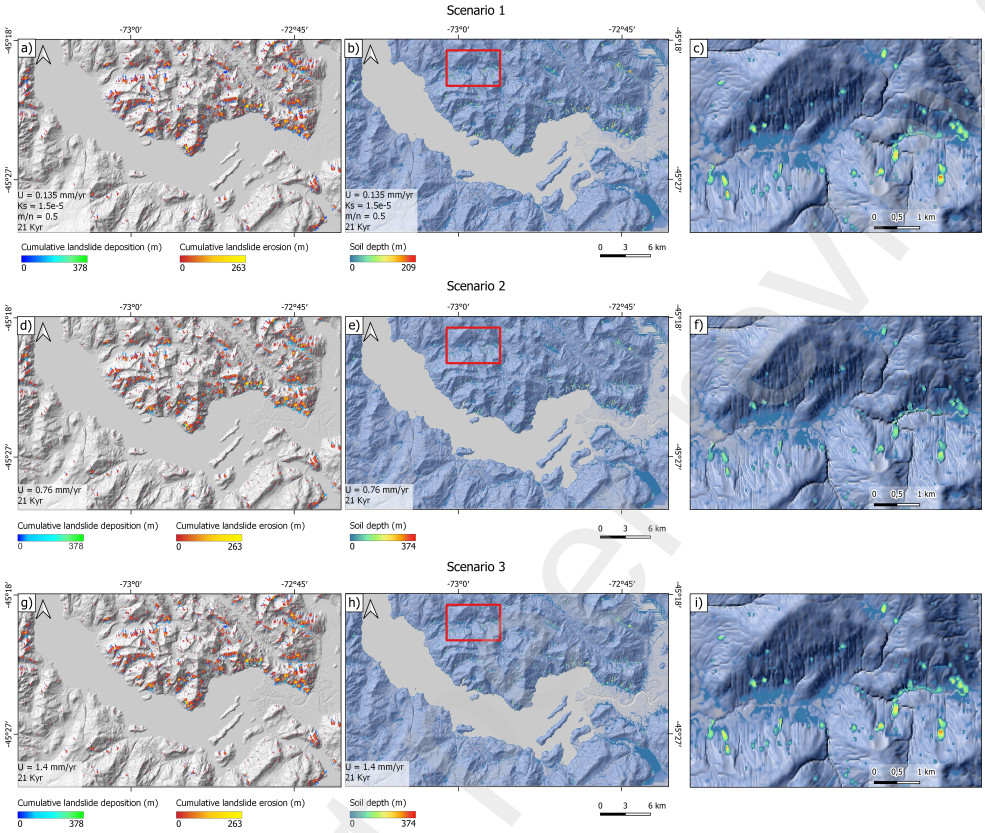

Figure 4: Left: Cumulative landslide erosion and cumulative deposition for scenarios with different rates of tectonic uplift (scenarios 1-3). Center: Soil depth at 21,000 simulation years for each scenario. Right: Region demarcated in the red box.

erodibility scenarios. However, it presents a downward trend compared to the current landscape with increased erodibility. The variability of this metric could be a consequence of the topography's variable roughness and the bedrock's differential erosion. We identified that the decrease in the m/n ratio induces the lowest k_{sn} of the evaluated scenarios (scenario 9) because of a non-linear incision that reduces the number of knickpoints regarding the other scenarios.

The excess of average topography in the simulated scenarios decreases regarding the current landscape. The average rock thickness in topographic excess increases slightly with increasing uplift (Figure 6). For its part, the increase in sediment erodibility triggers a general decrease in topographic

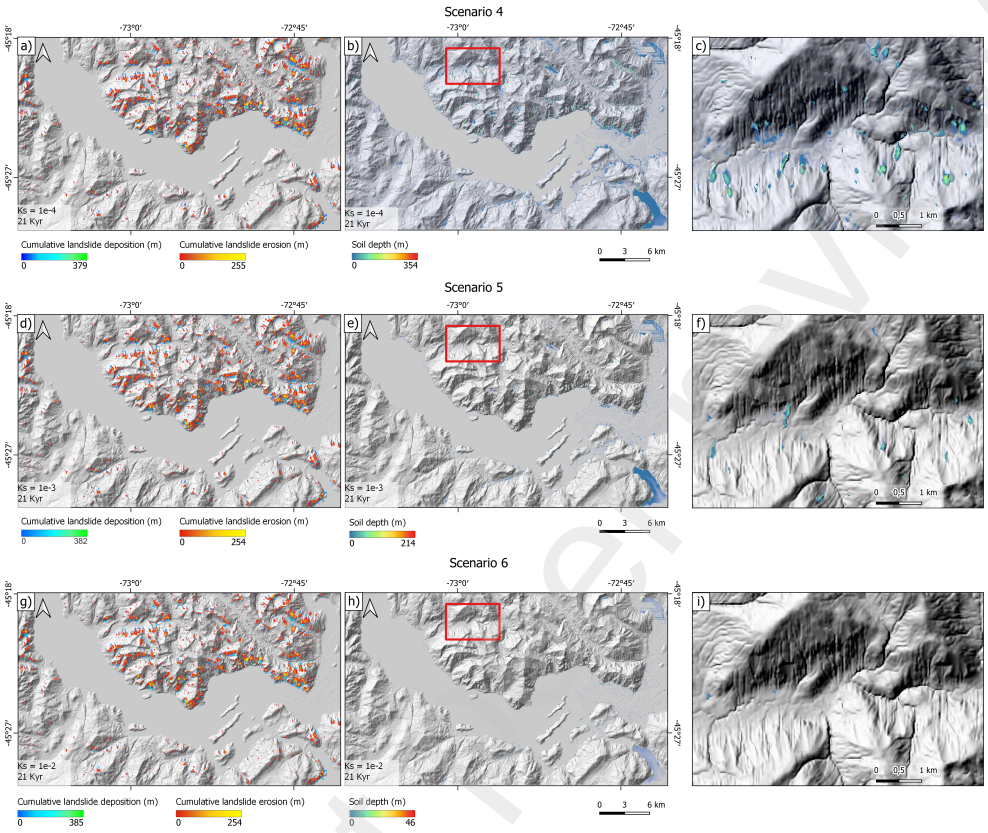

Figure 5: Left: cumulative landslide erosion and cumulative deposition for scenarios with different sediment erodibility conditions (scenarios 4-6). Center: Soil depth at 21,000 simulation years for each scenario. Right: Region demarcated in the red box.

excess. We highlight the impact of the decrease in the m/n ratio that effectively drives the slopes toward their threshold angle. According to our analysis, average elevation changes increase proportionally to the uplift rate, causing an average landscape growth of over 20 m (Figure 6; scenario 3). The increase in the sediment's erodibility and the decrease in the m/n ratio induce an average loss of relief of up to 40 m (Figure 6; scenario 9). There is a clear difference in the spatial distribution of topographic changes for the simulated scenarios (Figure 7). In general, the most significant topographic loss areas are linked to landslide erosion, while the highest topographic growth is associated with landslide deposits that remain on the slopes. Likewise, the valleys and plains show an increase in relief because of sedimentary filling

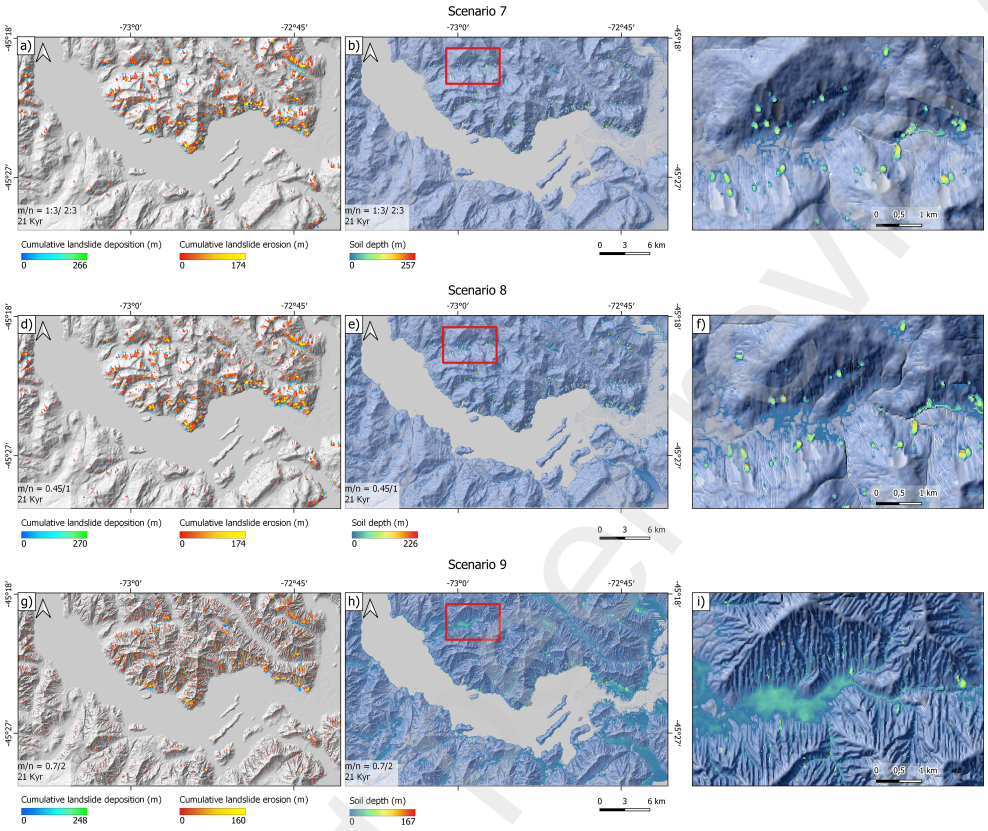

Figure 6: Left: cumulative landslide erosion and cumulative deposition for scenarios with different m/n ratios (scenarios 6-9). Center: Soil depth at 21,000 simulation years for each scenario. Right: Region demarcated in the red box.

due to landslides and fluvial dynamics.

According to our topographic classification, all the models have spatial proportions of heterogeneous landforms, mainly highlighting the slope, ridge, valley, and hollow types. We detected that the increase in the uplift rate (scenarios 1-3) causes an increase in spur and slope landforms and a decrease in valleys regarding the initial landscape (scenario 0). Variations in sediment erodibility generate a minimal increase in ridge-like landforms (scenarios 4-6). The decrease in m/n ratios reduces slope and increases ridge and valley-type landforms (scenario 9). According to the results, we obtained essential differences in terms of the variability of landforms in the uplift scenarios and m/n ratios. The K_s scenarios (scenarios 4-6) practically do not reflect

significant differences (Figure 7).

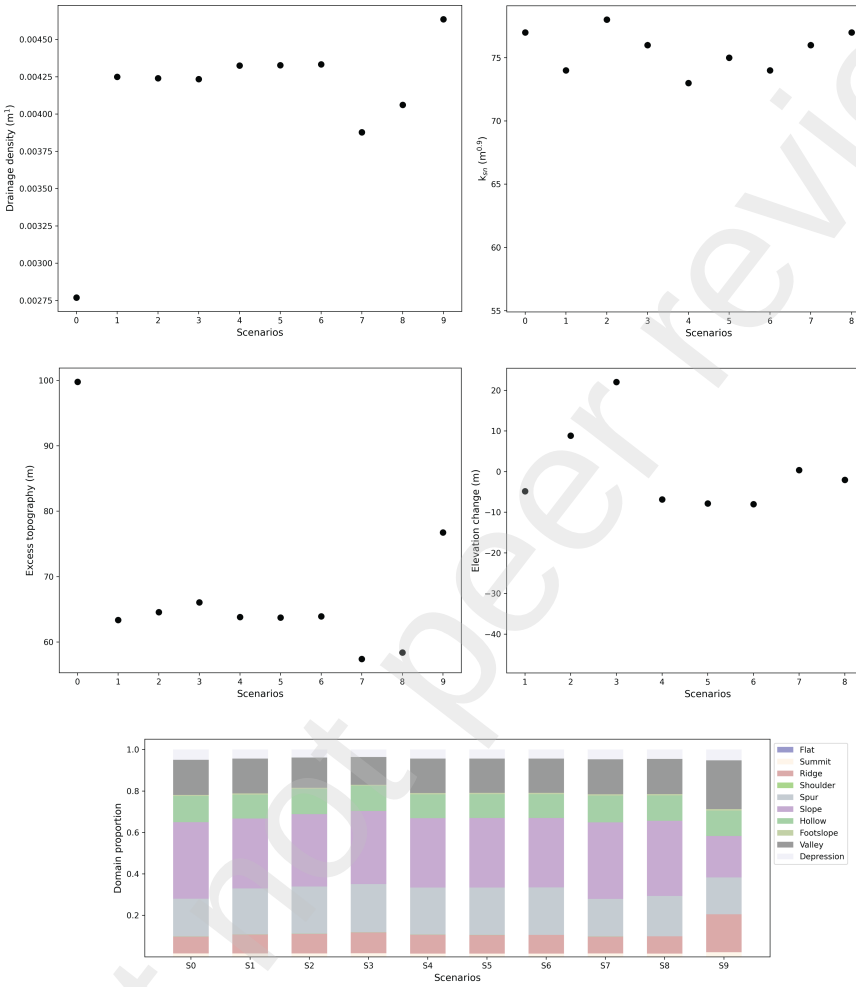

Figure 7: Analysis of topographic changes for the final simulated landscape and the current one (Scenario 0). A) Drain density. B) Average k_{sn}. C) Excess average topography. D) Average elevation changes.

5. Discussion

In this study, we analyzed the dynamics of sediments following a seismic event using a hybrid model which considered erosion by landslides and

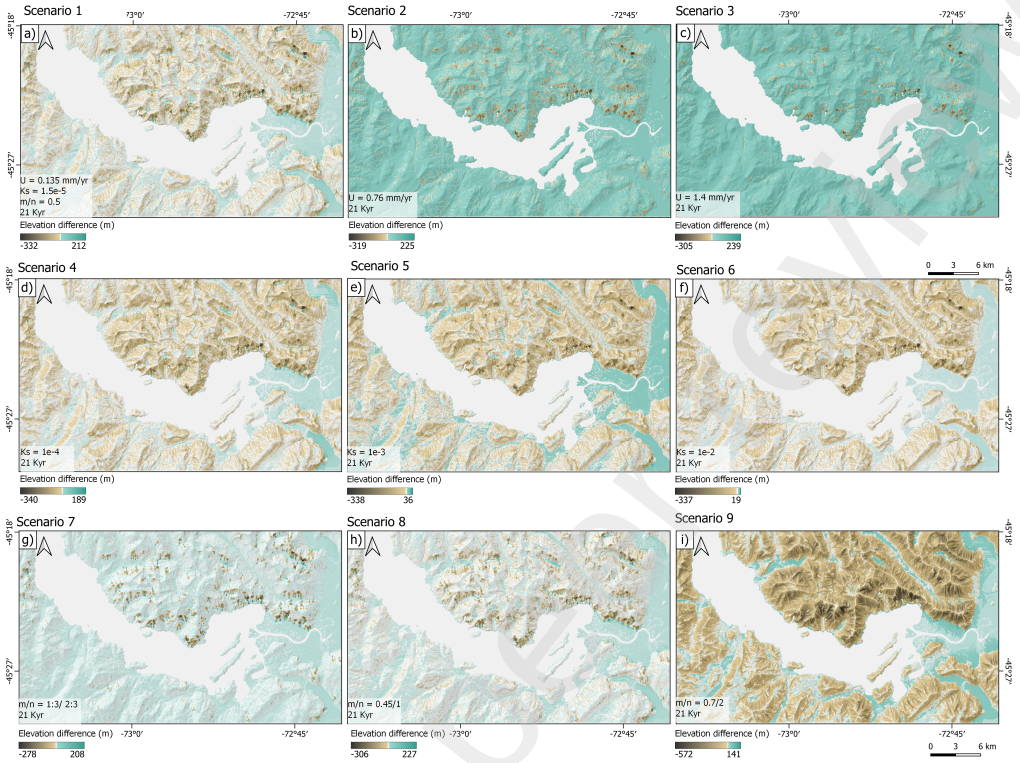

Figure 8: Elevation changes for each scenario after 21,000 years of simulation with respect to the current landscape.

subsequent fluvial transport. The study area was selected for different reasons; 1) there is a spacial inventory of landslides associated with the Aysén earthquake, 2) there is a historical record of earthquakes associated with the LOFS in the Aysén Fjord, 3) we have information about the period of the landslides induced by seismic activity, 4) this is an almost glacier-free area, with only small isolated bodies of ice.

Our experiments indicate that landslide-derived sediments can remain in mountains for centuries, this is consistent with observations made in epicentral areas of large earthquakes that have helped improve understanding of sediment permanence in mountain systems after of an earthquake (Francis et al., 2022; Wang et al., 2015; Hovius et al., 2011; Wang et al., 2015; Dai et al., 2021). According to our analysis, the permanence of landslide-derived deposits is directly related to model parameterization. For example, we note that high sediment erodibility conditions substantially reduce the volume of

deposits throughout the region (Figure 3, 5; scenario 6). We identified that the increase in the fluvial incision leads the slopes continuously towards their threshold angle, demonstrating a strong coupling between incision and landslides that substantially increases sediment production and the sediment load of the valleys (3, 5; scenario 9).

We identified that the landslides closest to the fluvial networks could interrupt the channels, generating morphological changes such as the displacement of the drainage incision zone or being evacuated by fluvial action depending on the model's parameterization. This dynamic has been documented in field observations (Hewitt, 2006). The landslides on the slopes are less effective in transferring sediments toward the fluvial channels, remaining on the slopes. Our results are consistent with analyzes carried out in other mountainous regions, where the connection of landslides to the channel has been found to regulate sediment transport after large earthquakes. Previous studies have observed that sediments on slopes farthest from the fluvial network are not available for transport in the short term (Li et al., 2016; Dai et al., 2021). In our simulations, we explicitly observe that channel avulsion is a standard process (Figure A.10), as it has been identified in real cases (Korup, 2004) and also by natural experiments (Campforts et al., 2022). However, increases in sediment erodibility strongly limit this type of process (Figure S2 in the supporting information). Finally, we believe that the tendency of the sediments to move towards the fjord is consistent with the stratigraphic record of the last 12,000 years (Wils et al., 2018).

Regarding the changes in the landscape at the scale of millennia in response to erosion by landslides and fluvial incisions, we identified that there is an increase in drainage density in all the simulated scenarios compared to the current landscape. Variations in the rate of uplift and erodibility have practically no impact on the formation of new drainage networks (Figure 7). In previous experimental models, they have detected that the increase in drainage density because of tectonic uplift is apparent (Campforts et al., 2022). However, in our study, we could not identify these patterns. We believe this is possible because of the reduced simulation times we used in our study that capture a limited dynamism of the landscape. We identified a different trend when decreasing the m/n ratios (scenario 9), which causes a substantial increase in drainage density. In this sense, our results are consistent with the studies that describe the importance of a non-linear incision in the evolution of landscapes (Lague, 2014).

The k_{sn} index presents a non-linear behavior. We believe that high k_{sn}

values reflect the formation of knickpoints because of increased uplift and sediment dynamics. The disappearance of knickpoints because of the increased incision is apparent by reducing the m/n ratios. According to our results, the final simulated landscape for each scenario shows a reduction in the average excess topography regarding the initial landscape. The increase in the coefficient n causes the persistence of a more unstable landscape over time since the development of drainage and incision leads the slopes permanently to their threshold angle. For this reason, scenario 9 reaches an average relief loss of up to 40 meters and has the highest excess relief values of the simulated scenarios (Figure 6). The differences in elevation between the simulated landscape and the current one is evidence of how erosion-deposition dynamics determine the areas where the relief decreases or grows. In this sense, parameterization's effects are notorious in each scenario's final response (Figure 7). It is important to note that, in our approach, we do not include the effect of characteristic post-seismic uplift in shallow (Parker et al., 2011; Li et al., 2018) earthquakes. We assume that the topographic changes associated with the seismic cycle are linked to landslides and derived deposits.

According to our terrain classification, changes in the parameterization influence the shapes of the final landscape of each scenario because of variable erosion and deposition rates. For example, recent studies have analyzed the role of deposits, and their impacts on the landscape (Ouimet et al., 2007; Roback et al., 2018; Shobe et al., 2021) finding that boulders derived from landslides can influence the transient fit and steady-state shape of the landscape (Shobe et al., 2021). Our results support the impact of these sediment clusters on the evolution of the landscape, driving the formation of new landforms, mainly in forming lateral ridges on the slopes (spur-type landforms). This reinforces that landslides are not only an erosion agent that regulates the growth of the relief (Li et al., 2014), but also can drive constructive landforms and be considered a formation process (Crozier, 2010). The increase in fluvial incisions combined with erosion by landslides favors the formation of new valleys and the widening of existing valleys (Figure S1 in the supporting information). According to our results, the geomorphological effects of landslides coupled with the incision can generate a noticeable impact at shorter time scales than previously documented in natural experiments (Campforts et al., 2022).

Our simulations show that the landslides are concentrated in preferential zones of the mountainous block, even sharing a common area of origin in different periods of time (Figures 4-6). In previous studies, it has been

identified that the reactivation of old landslides is frequent after earthquakes (Guo et al., 2020; Wasowski et al., 2021).

In the Andes' geological history, landslides' role in landscape formation is still poorly understood; we believe that landscape evolution models are a fundamental tool to address this gap. Approaches of this style can complement previous investigations that have evaluated the spatial patterns of rock slides in Andean Patagonia (Pánek et al., 2021, 2022). For example, the reverse topographic construction (Barnhart et al., 2020) could broaden the understanding of these processes in future analyses. In our study, lateral fluvial erosion is not considered, although landslides seem to control this dynamic. In the future, it will be crucial to incorporate the impact of drainage, as suggested by numerical experiments (Kwang et al., 2021). We also believe that future studies should consider the geological domain heterogeneity associated with rock type, as previously recommended (Campforts et al., 2020b). According to our results, in this region there will be an important control of the LOFS in the erosion of the landscape given its role in the superficial seismic cycle. In future research, it will be crucial to work on the incorporation of LOFS fault traces and thus represent the heterogeneity of cortical stress in the modeling domain.

Finally, we propose using these models to help evaluate threats in mountainous basins where landslides are predominantly geomorphological processes. However, more developments are needed to have reference data to establish the periodicity of the triggering events, the availability of geomechanical parameters, and the approximate rates of sediment transport, reducing the scenarios. In the same way, the landscape's response in the different scenarios suggests the need to restrict the values of the constants K, m, and n in the Andes. Although there have been efforts to understand the behavior of these parameters at a global level, unfortunately, the Andes lacks this information (Harel et al., 2016).

6. Conclusions

We use the HyLands-Landlab landscape evolution model to understand the role of earthquake-induced landslides and fluvial incisions in the landscape of northern Andean Patagonia through nine scenarios. We analyze the long-term effects on the landscape under idealized conditions of ten 2100-year seismic cycles based on the LOFS seismic history in the Aysen Fjord. Based on our results, we believe that landslide erosion is a fundamental process in

landscape evolution and sediment production. We identify that landslide-derived deposits induce the formation of transient landscape forms that can regulate fluvial incision at scales of thousands of years. Our results suggest that the parameterization causes essential changes in the evolutionary trajectory of the landscape in the evaluated time scale and is visible in multiple topographic metrics. We highlight that low m/n ratios can generate a final landscape response substantially different from the other scenarios since the slopes are constantly driven towards their threshold angle, intensifying the interaction between landslide erosion and fluvial incision. Based on our results and the historical record of the Aysén Fjord, we can infer an essential control of LOFS on landscape erosion and sediment production that had not been previously studied with this approach. Consistent with the results of our analysis, we believe that landscape evolution models are a powerful tool to explain sediment load contributions induced by large earthquakes on scales of thousands of years. Similarly, they can help improve our understanding of landslides' role in the Andes' evolutionary history. However, to limit the number of scenarios, it is essential to advance the erodibility's understanding and incision parameters of the current power law in the Andes and local geomechanical information. Finally, we believe that implementing landscape evolution models can help to understand landslide dynamics in other Andean basins exposed to these geomorphological processes.

Appendix A.

Conflict of interest

The authors declare that they have no conflict of interest.

Data Availability

The SRTM DEM used to obtain the morphometric and hydrological variables is publicly accessible at `https://earthexplorer.usgs.gov/` (last accessed on 15 October 2021), download platform of the U.S. Geological Survey (USGS). Landlab is completely accessible from its official repository on GitHub, `https://landlab.github.io` (last access on 10 march 2022). The source code for HyLands 1.0 (Campforts et al., 2020a) is available at `https://github.com/BCampforts/topotoolbox` (last access on 10 march 2022). The Landlab implementation of the HyLands 1.0 landslide

component is accessible at https://github.com/landlab/landlab/tree/master/landlab/components/bedrock_landslider (last access on 10 march 2022). The SPACE 1.0 component used to model fluvial erosion is accessible athttps://github.com/landlab/landlab/tree/master/landlab/components/space (last access on 10 march 2022).

Acknowledgements

We are funded by the Chilean Science Council (ANID) through the Program of International Cooperation (PII-180008), Water Research Center For Agriculture and Mining, CRHIAM (ANID/FONDAP/15130015), PATSER (ANID/R20F0002), and Anillo (ACT210080).

References

Barnhart, K.R., Tucker, G.E., Doty, S.G., Shobe, C.M., Glade, R.C., Rossi, M.W., Hill, M.C., 2020. Inverting topography for landscape evolution model process representation: 1. conceptualization and sensitivity analysis. Journal of Geophysical Research: Earth Surface 125. doi:10.1029/2018JF004961.

Blöthe, J.H., Korup, O., Schwanghart, W., 2015. Large landslides lie low: Excess topography in the himalaya-karakoram ranges. Geology 43, 523–526. URL: http://pubs.geoscienceworld.org/geology/article/43/6/523/131903/Large-landslides-lie-low-Excess-topography-in-the, doi:10.1130/G36527.1.

Booth, A.M., Roering, J.J., Rempel, A.W., 2013. Topographic signatures and a general transport law for deep-seated landslides in a landscape evolution model. Journal of Geophysical Research: Earth Surface 118, 603–624. doi:10.1002/jgrf.20051.

Broeckx, J., Rossi, M., Lijnen, K., Campforts, B., Poesen, J., Vanmaercke, M., 2020. Landslide mobilization rates: A global analysis and model. Earth-Science Reviews 201, 102972. URL: https://linkinghub.elsevier.com/retrieve/pii/S0012825219302557, doi:10.1016/j.earscirev.2019.102972.

Campforts, B., Shobe, C.M., Overeem, I., Tucker, G.E., 2022. The art of landslides: How stochastic mass wasting shapes topography and influences landscape dynamics. Journal of Geophysical Research: Earth Surface 127. URL: https://onlinelibrary.wiley.com/doi/10.1029/2022JF006745, doi:10.1029/2022JF006745.

Campforts, B., Shobe, C.M., Steer, P., Vanmaercke, M., Lague, D., Braun, J., 2020a. Hylands 1.0: a hybrid landscape evolution model to simulate the impact of landslides and landslide-derived sediment on landscape evolution. Geoscientific Model Development 13, 3863–3886. URL: https://gmd.copernicus.org/articles/13/3863/2020/, doi:10.5194/gmd-13-3863-2020.

Campforts, B., Vanacker, V., Herman, F., Vanmaercke, M., Schwanghart, W., Tenorio, G.E., Willems, P., Govers, G., 2020b. Parameterization of river incision models requires accounting for environmental heterogeneity: insights from the tropical andes. Earth Surface Dynamics 8, 447–470. URL: https://esurf.copernicus.org/articles/8/447/2020/, doi:10.5194/esurf-8-447-2020.

Carretier, S., Martinod, P., Reich, M., Godderis, Y., 2016. Modelling sediment clasts transport during landscape evolution. Earth Surface Dynamics 4, 237–251. doi:10.5194/esurf-4-237-2016.

Cembrano, J., Hervé, F., Lavenu, A., 1996. The liquiñe ofqui fault zone: a long-lived intra-arc fault system in southern chile. Tectonophysics 259, 55–66.

Champel, B., 2002. Growth and lateral propagation of fault-related folds in the siwaliks of western nepal: Rates, mechanisms, and geomorphic signature. Journal of Geophysical Research 107. doi:10.1029/2001jb000578.

Conrad, O., Bechtel, B., Bock, M., Dietrich, H., Fischer, E., Gerlitz, L., Wehberg, J., Wichmann, V., Böhner, J., 2015. System for automated geoscientific analyses (saga) v. 2.1.4. Geoscientific Model Development 8, 1991–2007. doi:10.5194/gmd-8-1991-2015.

Crozier, M.J., 2010. Landslide geomorphology: An argument for recognition, with examples from new zealand. Geomorphology 120, 3–15. doi:10.1016/j.geomorph.2009.09.010.

Culmann, K., 1875. Die graphische statik.

Dai, L., Scaringi, G., Fan, X., Yunus, A.P., Liu-Zeng, J., Xu, Q., Huang, R., 2021. Coseismic debris remains in the orogen despite a decade of enhanced landsliding. Geophysical Research Letters 48, 1–11. doi:10.1029/2021GL095850.

Davy, P., Lague, D., 2009. Fluvial erosion/transport equation of landscape evolution models revisited. Journal of Geophysical Research: Solid Earth 114. doi:10.1029/2008JF001146.

Densmore, A.L., Ellis, M.A., Anderson, R.S., 1998. Landsliding and the evolution of normal-fault-bounded mountains. Journal of Geophysical Research: Solid Earth 103, 15203–15219. URL: http://doi.wiley.com/10.1029/98JB00510, doi:10.1029/98JB00510.

Dulanya, Z., Gallen, S.F., Kolawole, F., Williams, J.N., Wedmore, L.N., Biggs, J., Åke Fagereng, 2022. Knickpoint morphotectonics of the middle shire river basin: Implications for the evolution of rift interaction zones. Basin Research doi:10.1111/bre.12687.

Fan, X., Scaringi, G., Korup, O., West, A.J., van Westen, C.J., Tanyas, H., Hovius, N., Hales, T.C., Jibson, R.W., Allstadt, K.E., Zhang, L., Evans, S.G., Xu, C., Li, G., Pei, X., Xu, Q., Huang, R., 2019. Earthquake-induced chains of geologic hazards: Patterns, mechanisms, and impacts. Reviews of Geophysics 57, 421–503. doi:10.1029/2018RG000626.

Francis, O., Fan, X., Hales, T., Hobley, D., Xu, Q., Huang, R., 2022. The fate of sediment after a large earthquake. Journal of Geophysical Research: Earth Surface 127, 1–19. URL: https://onlinelibrary.wiley.com/doi/10.1029/2021JF006352, doi:10.1029/2021JF006352.

Guo, C., Zhang, Y., Li, X., Ren, S., Yang, Z., Wu, R., Jin, J., 2020. Reactivation of giant jiangdingya ancient landslide in zhouqu county, gansu province, china. Landslides 17, 179–190. doi:10.1007/s10346-019-01266-9.

Harel, M.A., Mudd, S., Attal, M., 2016. Global analysis of the stream power law parameters based on worldwide 10be denudation rates. Geomorphology 268, 184–196. URL: https://linkinghub.elsevier.com/retrieve/pii/S0169555X16303907, doi:10.1016/j.geomorph.2016.05.035.

Hervé, F., Fuentes, F.J., Calderón, M., Fanning, M., Quezada, P., Pankhurst, R., Rapela, C., 2017. Ultramafic rocks in the north patagonian andes: is their emplacement associated with the neogene tectonics of the liquiñe–ofqui fault zone? Andean Geology 44, 1. URL: http://www.andeangeology.cl/index.php/revista1/article/view/V44n1-a01, doi:10.5027/andgeoV44n1-a01.

Hewitt, K., 2006. Disturbance regime landscapes: Mountain drainage systems interrupted by large rockslides. Progress in Physical Geography 30, 365–393. doi:10.1191/0309133306pp486ra.

Hovius, N., Meunier, P., Lin, C.W., Chen, H., Chen, Y.G., Dadson, S., Horng, M.J., Lines, M., 2011. Prolonged seismically induced erosion and the mass balance of a large earthquake. Earth and Planetary Science Letters 304, 347–355. doi:10.1016/j.epsl.2011.02.005.

Hovius, N., Stark, C.P., Allen, P.A., 1997. Sediment flux from a mountain belt derived by landslide mapping. Geology 25, 231. URL: https://pubs.geoscienceworld.org/geology/article/25/3/231-234/206598, doi:10.1130/0091-7613(1997)025<0231:SFFAMB>2.3.CO;2.

Jasiewicz, J., Stepinski, T.F., 2013. Geomorphons — a pattern recognition approach to classification and mapping of landforms. Geomorphology 182, 147–156. doi:10.1016/j.geomorph.2012.11.005.

Jeandet, L., Steer, P., Lague, D., Davy, P., 2019. Coulomb mechanics and relief constraints explain landslide size distribution. Geophysical Research Letters 46, 4258–4266. doi:10.1029/2019GL082351.

Korup, O., 2004. Landslide-induced river channel avulsions in mountain catchments of southwest new zealand. Geomorphology 63, 57–80. URL: https://linkinghub.elsevier.com/retrieve/pii/S0169555X04000959, doi:10.1016/j.geomorph.2004.03.005.

Korup, O., Densmore, A.L., Schlunegger, F., 2010. The role of landslides in mountain range evolution. Geomorphology 120, 77–90. URL: http://dx.doi.org/10.1016/j.geomorph.2009.09.017, doi:10.1016/j.geomorph.2009.09.017.

Kwang, J.S., Langston, A.L., Parker, G., 2021. The role of lateral erosion in the evolution of nondendritic drainage networks to dendricity and the persistence of dynamic networks. Proceedings of the National Academy of Sciences 118. doi:10.1073/pnas.2015770118.

Lague, D., 2014. The stream power river incision model: Evidence, theory and beyond. Earth Surface Processes and Landforms 39, 38–61. doi:10.1002/esp.3462.

Lai, J., Anders, A.M., 2018. Modeled postglacial landscape evolution at the southern margin of the laurentide ice sheet: Hydrological connection of uplands controls the pace and style of fluvial network expansion. Journal of Geophysical Research: Earth Surface 123, 967–984. doi:10.1029/2017JF004509.

Larsen, I.J., Montgomery, D.R., 2012. Landslide erosion coupled to tectonics and river incision. Nature Geoscience 5, 468–473. doi:10.1038/ngeo1479.

Lastras, G., Amblas, D., Calafat, A.M., Canals, M., Frigola, J., Hermanns, R.L., Lafuerza, S., Longva, O., Micallef, A., Sepúlveda, S.A., Vargas, G., Batist, M.D., Daele, M.V., Azpiroz, M., Bascuñán, I., Duhart, P., Iglesias, O., Kempf, P., Rayo, X., 2013. Landslides cause tsunami waves: Insights from aysén fjord, chile. Eos, Transactions American Geophysical Union 94, 297–298. URL: https://agupubs.onlinelibrary.wiley.com/doi/abs/10.1002/2013EO340002, doi:https://doi.org/10.1002/2013EO340002, arXiv:https://agupubs.onlinelibrary.wiley.com/doi/pdf/10.1002/2013EO340002.

Li, C., Wang, M., Liu, K., Xie, J., 2018. Topographic changes and their driving factors after 2008 wenchuan earthquake. Geomorphology 311, 27–36. doi:10.1016/j.geomorph.2018.03.019.

Li, G., West, A.J., Densmore, A.L., Hammond, D.E., Jin, Z., Zhang, F., Wang, J., Hilton, R.G., 2016. Connectivity of earthquake-triggered landslides with the fluvial network: Implications for landslide sediment transport after the 2008 wenchuan earthquake. Journal of Geophysical Research: Earth Surface 121, 703–724. doi:10.1002/2015JF003718.

Li, G., West, A.J., Densmore, A.L., Jin, Z., Parker, R.N., Hilton, R.G., 2014. Seismic mountain building: Landslides associated with the 2008 wenchuan earthquake in the context of a generalized model for earthquake volume

balance. Geochemistry, Geophysics, Geosystems 15, 833–844. doi:10.1002/2013GC005067.

Milliman, J.D., Meade, R.H., 1983. World-wide delivery of river sediment to the oceans. The Journal of Geology 91, 1–21. URL: https://www.journals.uchicago.edu/doi/10.1086/628741, doi:10.1086/628741.

Naranjo, J.A., Arenas, M., Clavero, J., Muñoz, O., 2009. Mass movement-induced tsunamis: main effects during the patagonian fjordland seismic crisis in aisén (45 25's), chile. Andean Geology 36, 137–145.

Ouimet, W.B., Whipple, K.X., Royden, L.H., Sun, Z., Chen, Z., 2007. The influence of large landslides on river incision in a transient landscape: Eastern margin of the tibetan plateau (sichuan, china). Geological Society of America Bulletin 119, 1462–1476. URL: https://pubs.geoscienceworld.org/gsabulletin/article/119/11-12/1462-1476/125374, doi:10.1130/B26136.1.

Parker, R.N., Densmore, A.L., Rosser, N.J., Michele, M.D., Li, Y., Huang, R., Whadcoat, S., Petley, D.N., 2011. Mass wasting triggered by the 2008 wenchuan earthquake is greater than orogenic growth. Nature Geoscience 4, 449–452. doi:10.1038/ngeo1154.

Pánek, T., Březný, M., Harrison, S., Schönfeldt, E., Winocur, D., 2022. Large landslides cluster at the margin of a deglaciated mountain belt. Scientific Reports 12, 5658. URL: https://www.nature.com/articles/s41598-022-09357-9, doi:10.1038/s41598-022-09357-9.

Pánek, T., Březný, M., Kilnar, J., Winocur, D., 2021. Complex causes of landslides after ice sheet retreat: Post-lgm mass movements in the northern patagonian icefield region. Science of The Total Environment 758, 143684. URL: https://linkinghub.elsevier.com/retrieve/pii/S0048969720372156, doi:10.1016/j.scitotenv.2020.143684.

Roback, K., Clark, M.K., West, A.J., Zekkos, D., Li, G., Gallen, S.F., Chamlagain, D., Godt, J.W., 2018. The size, distribution, and mobility of landslides caused by the 2015 mw7.8 gorkha earthquake, nepal. Geomorphology 301, 121–138. URL: https://linkinghub.elsevier.com/retrieve/pii/S0169555X1630719X, doi:10.1016/j.geomorph.2017.01.030.

Schwanghart, W., Bernhardt, A., Stolle, A., Hoelzmann, P., Adhikari, B.R., Andermann, C., Tofelde, S., Merchel, S., Rugel, G., Fort, M., Korup, O., 2016. Repeated catastrophic valley infill following medieval earthquakes in the nepal himalaya. Science 351, 147–150. URL: https://www.science.org/doi/abs/10.1126/science.aac9865, doi:10.1126/science.aac9865.

Sepúlveda, S.A., Serey, A., Lara, M., Pavez, A., Rebolledo, S., 2010. Landslides induced by the april 2007 aysén fjord earthquake, chilean patagonia. Landslides 7, 483–492. URL: http://link.springer.com/10.1007/s10346-010-0203-2, doi:10.1007/s10346-010-0203-2.

Shobe, C.M., Tucker, G.E., Barnhart, K.R., 2017. The space 1.0 model: a landlab component for 2-d calculation of sediment transport, bedrock erosion, and landscape evolution. Geoscientific Model Development 10, 4577–4604. URL: https://gmd.copernicus.org/articles/10/4577/2017/, doi:10.5194/gmd-10-4577-2017.

Shobe, C.M., Turowski, J.M., Nativ, R., Glade, R.C., Bennett, G.L., Dini, B., 2021. The role of infrequently mobile boulders in modulating landscape evolution and geomorphic hazards. Earth-Science Reviews 220, 103717. URL: https://linkinghub.elsevier.com/retrieve/pii/S001282522100218X, doi:10.1016/j.earscirev.2021.103717.

Stock, J.D., Montgomery, D.R., 1999. Geologic constraints on bedrock river incision using the stream power law. Journal of Geophysical Research: Solid Earth 104, 4983–4993. doi:10.1029/98jb02139.

Stolle, A., Schwanghart, W., Andermann, C., Bernhardt, A., Fort, M., Jansen, J.D., Wittmann, H., Merchel, S., Rugel, G., Adhikari, B.R., Korup, O., 2019. Protracted river response to medieval earthquakes. Earth Surface Processes and Landforms 44, 331–341. doi:10.1002/esp.4517.

Thomson, S.N., Brandon, M.T., Tomkin, J.H., Reiners, P.W., Vásquez, C., Wilson, N.J., 2010. Glaciation as a destructive and constructive control on mountain building. Nature 467, 313–317. URL: http://www.nature.com/articles/nature09365, doi:10.1038/nature09365.

Tolorza, V., Mohr, C.H., Carretier, S., Serey, A., Sepúlveda, S.A., Tapia, J., Pinto, L., 2019. Suspended sediments in chilean rivers reveal low

postseismic erosion after the maule earthquake (mw 8.8) during a severe drought. Journal of Geophysical Research: Earth Surface 124, 1378–1397. doi:10.1029/2018JF004766.

Tucker, G.E., 2009. Natural experiments in landscape evolution. Earth Surface Processes and Landforms 34, 1450–1460. URL: http://doi.wiley.com/10.1002/esp.1730https://onlinelibrary.wiley.com/doi/10.1002/esp.1833, doi:10.1002/esp.1833.

Tucker, G.E., Whipple, K.X., 2002. Topographic outcomes predicted by stream erosion models: Sensitivity analysis and intermodel comparison. Journal of Geophysical Research: Solid Earth 107, ETG 1–1–ETG 1–16. doi:10.1029/2001JB000162.

Vargas, G., Rebolledo, S., Sepúlveda, S.A., Lahsen, A., Thiele, R., Townley, B., Padilla, C., Rauld, R., Herrera, M.J., Lara, M., 2013. Ruptura sísmica submarina, tectónica y volcanismo activo a lo largo de la falla liquiñe-ofqui e implicancias para el peligro sísmico en los andes patagónicos. Andean Geology 40, 141–171. doi:10.5027/andgeoV40n1-a07.

Villalobos, A., Easton, G., Maksymowicz, A., Ruiz, S., Lastras, G., Pascale, G.P.D., Agurto-Detzel, H., 2020. Active faulting, submarine surface rupture, and seismic migration along the liquiñe-ofqui fault system, patagonian andes. Journal of Geophysical Research: Solid Earth 125. doi:10.1029/2020JB019946.

Wang, J., Jin, Z., Hilton, R.G., Zhang, F., Densmore, A.L., Li, G., West, A.J., 2015. Controls on fluvial evacuation of sediment from earthquake-triggered landslides. Geology 43, 115–118. doi:10.1130/G36157.1.

Wasowski, J., McSaveney, M.J., Pisano, L., Gaudio, V.D., Li, Y., Hu, W., 2021. Recurrent rock avalanches progressively dismantle a mountain ridge in beichuan county, sichuan, most recently in the 2008 wenchuan earthquake. Geomorphology 374. doi:10.1016/j.geomorph.2020.107492.

Whittaker, A.C., 2012. How do landscapes record tectonics and climate? Lithosphere 4, 160–164. doi:10.1130/RF.L003.1.

Wils, K., Daele, M.V., Lastras, G., Kissel, C., Lamy, F., Siani, G., 2018. Holocene event record of aysén fjord (chilean patagonia): An interplay

of volcanic eruptions and crustal and megathrust earthquakes. Journal of Geophysical Research: Solid Earth 123, 324–343. doi:10.1002/2017JB014573.

Yanites, B.J., Tucker, G.E., Mueller, K.J., Chen, Y.G., 2010. How rivers react to large earthquakes: Evidence from central taiwan. Geology 38, 639–642. doi:10.1130/G30883.1.

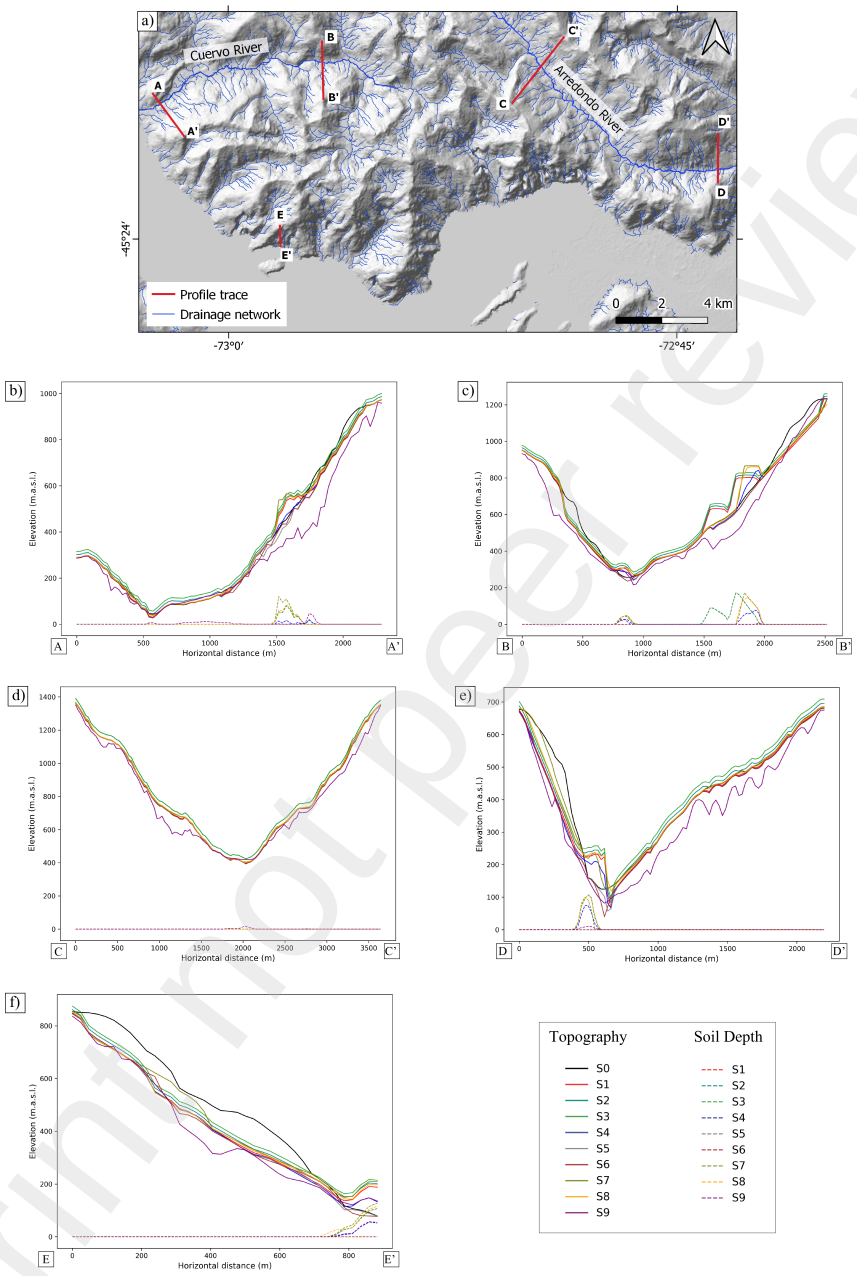

Figure A.9: Topographic and soil thickness profiles in two main rivers in the study area. In the profiles, we compare the simulated final landscape for each of the scenarios with the current one (S0). Solid lines represent the topography and the dashed lines represent the thickness of the soil. The location of the profiles is shown in (a). Profiles reflect how the coupling between landslides and fluvial incision change the morphology of the slopes and the channel under different conditions of uplift, erodibility and m/n ratios (b-c).

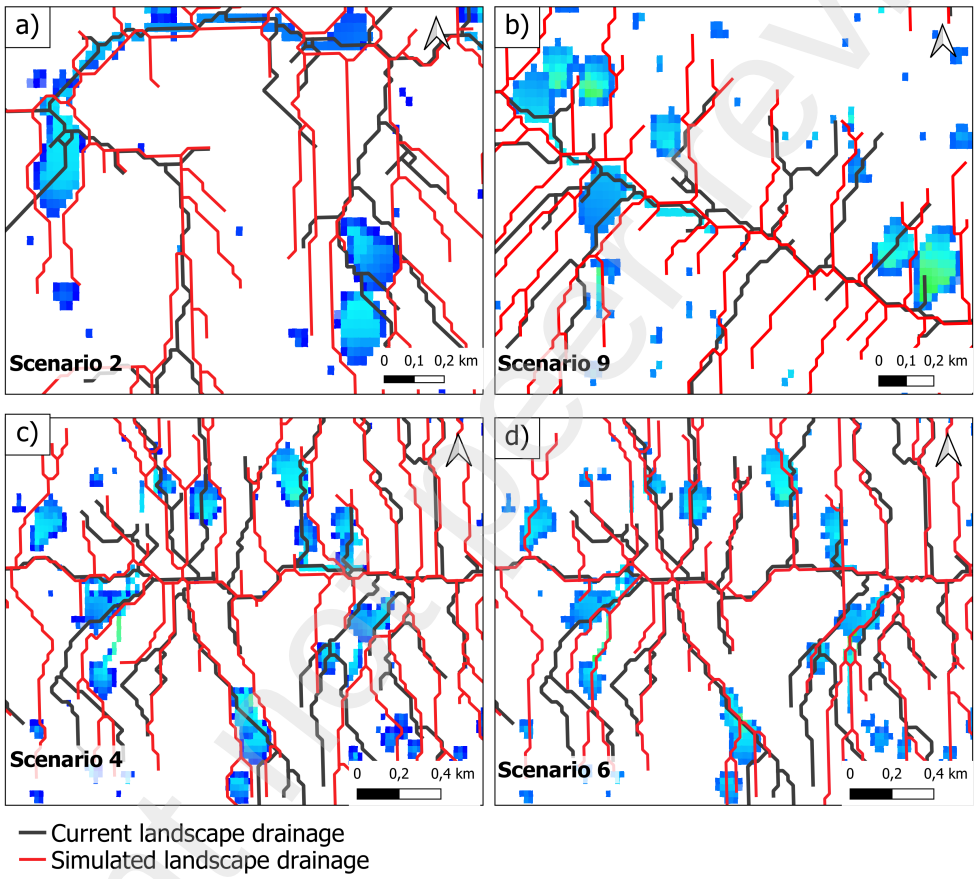

Figure A.10: Landslide-induced channel avulsion (a-c). High sediment erodibility limits the avulsion process (d).